International Conference on Space Optics—ICSO 2014

La Caleta, Tenerife, Canary Islands

7–10 October 2014

Wave-front sensing for space active optics: Rascasse project

Arnaud Liotard

Marc Bernot

Mikaël Carlavan

Frédéric Falzon

et al.

WAVE-FRONT SENSING FOR SPACE ACTIVE OPTICS: RASCASSE PROJECT

Arnaud Liotard[1], Marc Bernot[1], Mikaël Carlavan[1], Frédéric Falzon[1],
Thierry Fusco[2], Vincent Michau[2], Aurélie Montmerle-Bonnefois[2], Laurent Mugnier[2],
Céline Engel[3], Clément Escolle[3], Marc Ferrari[3], Emmanuel Hugot[3],
Thierry Bret-Dibat[4], David Laubier[4]

[1]Thales Alenia Space, Cannes-la-Bocca, France.
[2]Office National d'Etudes et de Recherches Aérospatiales (ONERA), Châtillon, France.
[3]Laboratoire d'Astrophysique de Marseille (LAM), France.
[4]Centre National d'Etudes Spatiales (CNES), Toulouse, France

I.   INTRODUCTION

I.1   Context

The payloads for Earth Observation and Universe Science are currently based on very stiff opto-mechanical structures with very tight tolerances. The introduction of active optics in such an instrument would relax the constraints on the thermo-mechanical architecture and on the mirrors polishing. A reduction of the global mass/cost of the telescope is therefore expected. Active optics is based on two key-components: the wave-front sensor and the wave-front corrector.

RASCASSE is a French acronym which stands for "Réalisation d'un Analyseur de Surface d'onde pour le Contrôle de miroirs Actifs Spatiaux sur Sources Etendues". This project aims at studying, implementing and testing Wave-Front Sensors which are intended to be installed in an active optics loop for very high resolution telescopes from space. It gathers Thales Alenia Space (TAS), ONERA and the Laboratoire d'Astrophysique de Marseille (LAM) with CNES support and expertise.

The most efficient solution to characterize the perturbation of an optical system is by putting a wave-front sensor close to the focal plane. Two technologies of Wave-Front Sensors have been selected for comparison within a space application as indicated above: the Shack-Hartmann sensor, which operates in conjugated pupil plane, and the Phase Diversity sensor, which operates in the focal plane. In this project, we propose to study and to adapt these two sensors, either to the case of a star, or to the case of extended scenes. As we consider here Earth orbiting imagers, these changing and complex scenes are most of the time acquired with micro-vibrations, and with a weak signal-to-noise ratio.

After a study-and-simulation phase of the two concepts, carried out by TAS and ONERA, we proceed to their validation on a dedicated active optics bench at LAM.

I.2   State-of-the art of the wave-front sensors for space applications

An active optics system is based on a device able to measure its optical performance, i.e. the residual aberrations. Several techniques are available to sense the wave front. The trade-off depends on the optical source and on the measurement conditions. In the case of space observation, measurement should be performed by using the observed scene, that is to say an extended structured unknown image. Moreover, measurement should be adapted to the acquisition mode and in particular to a potentially low level of flux.

Meanwhile extended sources have been considered with most of existing wave-front sensor (WFS) [1][2][3][4], demonstrations with Shack-Hartmann WFS [3], and with phase diversity WFS [4], are the most convincing.

Main works on Shack-Hartmann WFS, see Figure 1, with extended scene were performed in the frame of adaptive optics for sun imagery, [5][6][7]. Some systems based on this WFS are currently operational on sky [8]. Nevertheless, to the best of our knowledge this method has never been tested for space observation.
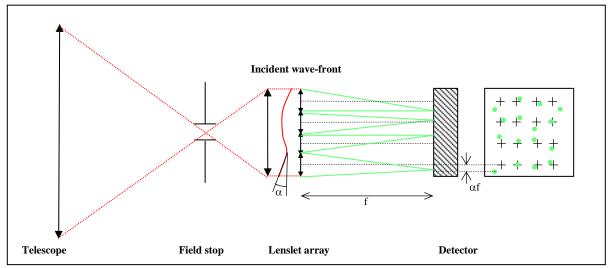
Figure 1 Principle of the Shack Hartmann wave-front sensor

   Phase Diversity, see Figure 2, was first proposed by Gonsalves in 1982 for wave front sensing in adaptive optics. Since 1990, this method is studied in the frame of astronomy. One of the main advantages of this method is its hardware simplicity. That is the reason why phase diversity was retained for measuring the spherical aberration of Hubble Space Telescope [9] or for the fine cophasing of JWST segments [10]. In these applications the object was known because it was a non-resolved star. Phase diversity could also be used for wave front sensing on an extended scene. It was the object of many experimental demonstrations in the case of monolithic telescopes [11]; or with segmented telescopes [12]. Different limitations linked with noise in acquired data were analysed [13][14]. Some algorithmic developments were leaded in parallel to optimize the noise reduction [15] or to reduce computation time for cophasing applications [16]. To be exhaustive, we should mention some tests with phase diversity in real time control of an adaptive optics system on extended scene for astronomy [17].
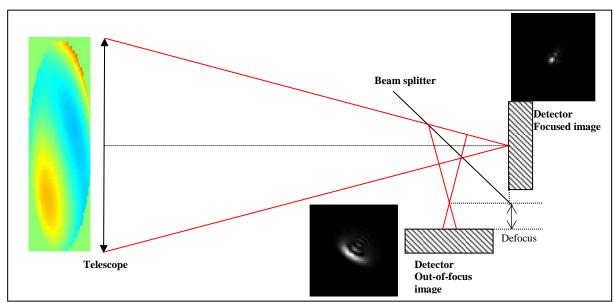

Figure 2 Principle of the Phase Diversity

   The RASCASSE project have been thought as a whole study gathering numerical simulations and experience of these two wave-front sensors: Shack-Hartmann, and phase diversity.

II. NUMERICAL MODELING AND SIMULATIONS

II.1 Study cases

The goal of the RASCASSE project is to explore all abilities of the WFS respectively to the observed scenes and to the WFE to be measured. In order to limit the number of possibilities in the sensitivity study, 5 scenarios split in two domains: lower aberrations (scenarios 1, 3 &5), and stronger aberrations (scenarios 2 &4).

Scenarios 1&2 are based on star acquisition. Static aberrations are declared unknown apart from the polishing errors. Scenario 1&2 differ in the amplitude of the aberrations for a parametric study. Scenario 1 corresponds to the lower aberrations case, and scenario 2 to the stronger aberrations one, see Figure 3.

Scenario 3 &4 consider extended and unknown scenes. Low frequency static aberrations which can be compensated have been compensated. It remains high frequency static aberrations and the dynamic aberrations. No assumption can be made on the aberrations. The full range of the dynamic aberrations is considered. As scenarios 1&2, scenario 3&4 differ in their amplitude. Scenario 3 has lower dynamic aberrations than scenario 4 and follows the scenario 1.

These four scenarios are summarized in the diagram presented in Figure 3. The 5th scenario constitutes the worst case. In this case the flight instrument acceptance testing is conducted on extended scene. All low frequency modes should be estimated on an extended scene.
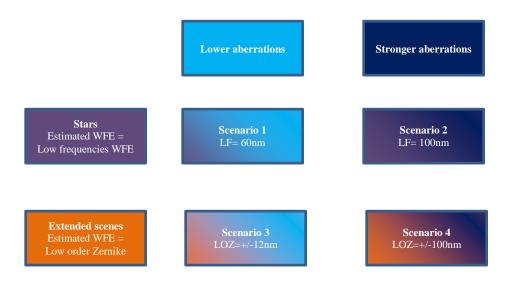
	Lower aberrations	Stronger aberrations
Stars Estimated WFE = Low frequencies WFE	**Scenario 1** LF= 60nm	**Scenario 2** LF= 100nm
Extended scenes Estimated WFE = Low order Zernike	**Scenario 3** LOZ=+/-12nm	**Scenario 4** LOZ=+/-100nm

Figure 3 RASCASSE study cases from #1 to #4

II.2 Simulation representativeness

Simulations parameters had been chosen to be as close as possible to the flight telescope. The f-number is fixed at 20 which is the value foreseen for the flight model. The considered extended scenes are provided by CNES. These scenes are aerial photographs acquired by the Pelican instrument. Pupil taken into account in the simulations presents a central obscuration and a spider representative of the space instrument. For phase-diversity, as in the flight detector, the acquired image is sub-sampled with a factor 2 with respect to the Shannon criterion.

WFE aberrations mainly come from the distortion of the "floppy" lightweight primary mirror. The gravity – release WFE map should be considered as unknown. Wave-front sensor performances are estimated in open-loop. The error function is the difference between the estimated WFE map and the initial WFE map.

II.3 Simulations results

The specification on the error in the estimations of the WFE is fixed at 10 nm for both modes. Results obtained with a full image chain model for the different WFS are gathered in Table 1. For further details, please refer to [18].The major difficulty encountered in this phase was the impact of the WFE high frequencies on the estimation of the low frequencies (LF). As we can see, accuracies are satisfying and compliant with specifications. Indeed performance on point wise object are better than 10 nm rms and estimation of low order

Zernike polynomials on extended scenes is better than 5nm. The WFS appear to be robust versus noise and image content.

Results obtained in scenario 1 are better than those obtained in scenario 5. WFS perform better on star than on extended scenes.

		Shack-Hartmann 8x8	Phase diversity ONERA	Phase diversity TAS
Scenario 1 LF=60nm rms	Star	5 nm	6 nm	<4nm
Scenario 2 LF=100nm rms	Star	10 nm	7 nm	<7nm
Scenario 3 low-order Zernike +/- 12nm	Nominal flux Range for various scenes	<2nm	Eqm_4 <1 nm for SNR_{mean} >10	<1nm for SNR_{mean} =25
	Low flux Range for various scenes	<2nm		< 3nm for SNR_{mean} =9
Scenario 4 low-order Zernike +/- 100nm	Nominal flux Range for various scenes	[3nm-20nm]	<5nm for SNR_{mean} >20	<5nm for SNR_{mean} =25
	Low flux Range for various scenes	[3nm-20nm]		[8nm-20nm] for SNR_{mean} =9
Scenario 5 LF=60nm rms	High flux Extended scene	8nm	10nm, for SNR > 50	8nm

Table 1 Summary of numerical simulations results.
Accuracy obtained in numerical simulations is fully compliant with system-specifications. Performances on star objects are better than 10 nm. Performances on extended scenes remain better than 5 nm per low-order Zernike mode. Considered WFS are globally robust against the noise and the image content.

WFS performances are very high in agreement with the system specifications for an open-loop behaviour. The main limitation found is the impact of the high frequencies in the low frequencies retrieval. The effect have been observed for both Shack-Hartmann and phase diversity. In the case of phase diversity, this phenomenon is more or less a coupling between the aberrations in the PSF space. For instance, separating 7th order spherical aberration from 5th order spherical aberration is not trivial. In the case of Shack-Hartmann WFS, physical phenomenon is different but the impact is quite the same. In presence of high aberrations, the WFE is bad sampled by the lenslet array. The assumption that wave front is flat inside a sub-pupil is no longer valid. Consequently, we do not observe a simple shift of the image but a PSF deformation.

III. EXPERIMENTAL TESTS

III.1   Experimental scenarios

Experimental scenarios are close the simulated ones. Slight modifications were performed in the WFE to be retrieved. In particular, we increase the amplitude to low-order Zernike polynomials in scenario 3 and polishing residuals are now considered as unknown. But the major issue to be tackled was to adapt the simulation scenario to experimental constraints. For instance, it was not possible to introduce a variable coma aberration.

III.2   Experimental breadboard

As in the simulation phase, the experimental set-up has been thought to be as representative as we can. The experimental F-number is equal to 25 which is a value close to the aperture of the space telescope. Images displayed for the extended scenes case are the same images used in the simulation phase and are provided by CNES. This images are displayed thanks to a micro-OLED device. Experimental pupil is a laser-machined carbon sheet. The pupil geometry is the same as the space telescope. Detector sampling and numerical aperture have been adjusted in the way to obtain, either a Shannon sampling, or a sub-sampling after pixel binning representative of the space instrument sampling.

Concerning the WFE maps, one of the lessons learnt during the simulation phase was the impact of high frequencies in the WFE map on the low frequency estimation. The second point is that we want to compare our estimation to an experimental reference. A deformable mirror was used previously on MADRAS bench to generate the WFE maps, [19], but cannot satisfy the RASCASSE requirements. Thus, we decided to emulate the WFE by etching the WFE map in a silica substrate – Silios technology. These maps are representative of aberrations such as polishing residuals, mechanical distortions and alignment losses. As these aberrations are difficult to predict, this WFE map cannot used a prior information for WFS. These scenarios lead to the definition of 7 phase masks to be machined:

- 1st phase mask: scenario 1 (HF+LF in case 1)
- 2nd phase mask: scenario 3bis (HF in the case 1 + coma)
- 3rd phase mask: scenario 3 (HF in case 2)
- 4th phase mask: scenario 2 (HF+BF in case 2)
- 5th phase mask: scenario 2bis (BF in case 2)
- 6th phase mask: scenario 4 (HF in case 2)
- 7th phase mask: neutral mask used to evaluate the optical bench aberrations

In addition to these phase masks, a lens is placed on a translation stage to complete the aberration panel by introducing a variable defocus.

Shack-Hartmann sensor and Phase diversity sensor were designed and experimentally implemented. A photograph of the optical breadboard located at LAM is shown in Figure 4. For more details, please read reference [20] in these conference proceedings.
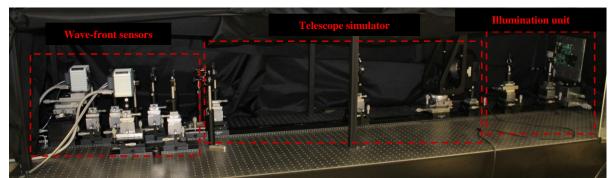

Figure 4 Photograph of the RASCASSE breadboard at LAM
RASCASSE breadboard is dedicated for wave-front sensor characterization.
This smart set-up is fully representative of the space telescope.

The goal of the RASCASSE experiment is to work in open loop. For that, we choose to compare absolute value of the WFE in order to characterize the WFS performances. However as the bench aberrations are not known with the required accuracy, WFS would not evaluate the real absolute value of the WFE. In phase-diversity, WFE measurement is a difference of two absolute WFE measurements (subtraction of bench

aberrations). In the Shack-Hartmann case, measurement is relative: centroid positions are registered in the case of the neutral mask, and centroid shift is used to retrieved the WFE maps.

III.3   Experimental results

The phase masks acceptance showed us a negligible difference with the specifications. Thanks to this efficient breadboard high quality raw images have been delivered: low stray light and very weak detector noise. Criterion for the experimental phase for all scenarios is fixed to 20 nm rms. Goal value is 10 nm rms. No major issues have been encountered during measurements exploitation. The following table shows the residual error between the estimated WFE and the etched WFE. For further details, please refer to [18].

		Shack-Hartmann 10x10	Phase diversity ONERA	Phase diversity TAS
Scenario 1 LF=80nm rms	Star	13 nm	14 nm	12 nm
Scenario 2 LF=140nm rms	Star	18 nm	12 nm	13nm
Scenario 3 low-order Zernike +/- 100nm	Extended scene High flux	<1 nm	<1 nm	<1 nm
	Extended scene Low flux	<1nm (SNR=63) 2nm (SNR=20)		<1 nm (SNR=25) <3 nm (SNR=9)
Scenario 4 low-order Zernike +/- 100nm	Extended scene High Flux	<1 nm		<2 nm
	Extended scene Low flux	<1nm (SNR=63) 2nm (SNR=20)	<2 nm (SNR=26) <1 nm (SNR=12) <4 nm (SNR=6)	< 2 nm (SNR=25) <3 nm (SNR=9)
Scenario 5– LF=80nm rms	Extended scene High Flux	16 nm until Z_{21}	16 nm until Z_{14}	16 nm until Z_{14}

Table 2 Summary of the experimental results

Performances on stars are in the 10-20 nm rms range, which is compliant with specifications but beyond the 10 nm goal value. Low-order Zernike modes are retrieved on extended scenes with an accuracy around 5nm rms fully compliant with the specifications even with the goal value.

The analysis of this table teaches us that experimental performances of the Shack-Hartmann WFE and of the phase diversity are, on the whole, positive. The estimation of the low order Zernike coefficient on extended scenes are around 5 nm rms, better than the goal specified value. Performances on stars are in the 10–20 nm rms range, compliant with the specifications but beyond the goal value.

IV. COMPARISON BETWEEN NUMERICAL SIMULATIONS AND EXPERIMENTAL RESULTS

The comparison between experimental results presented in Table 2 and the simulation results gathered in the Table 1 teaches us that performances with extended scene are in agreement. Experimental results on stars are satisfying but seem to be less good than the performances obtained in the simulation phase. Obtaining better results in simulations than in experiment is quite logic. In the numerical simulation, image formation model is fully mastered; in experiment, many physical phenomena can affect the image formation. Many parameters cannot be predicted and are estimated by the algorithms. This gap remains at the present time unexplained.

The first lead we can pursue is the WFE stability. This stability is essential because the bench aberrations are subtracted a posteriori. The second lead is the global aberrations of the bench (chromatic and field aberrations). The field aberrations can affect significantly the WFE measurement in extended scenes. In consequence we recommend to perform complementary measurements in order to better understand this residual gap between simulations and experiment.

V. CONCLUSION

The RASCASSE project lasted 24 months. In this timescale, a whole study gathering numerical simulations and experimental characterization of two Wave-front sensors has been realized. Performances of Shack-Hartmann WFS and of phase-diversity were simulated in open loop, and are in agreement with the system-specifications. The estimation of the low-order Zernike coefficients on extended scenes are around 5 nm rms. Performances on stars are better than 10 nm rms.

An experimental set-up is assembled and aligned. This bench is representative of the main parameters of a space telescope :observed objects, WFE to be retrieved, pupil geometry, numerical aperture, etc. Shack-Hartmann sensor and Phase diversity sensor were experimentally implemented.

Results on extended scenes are in the 5nm-per-mode class in agreement with simulations. On a point source like object, WFS get an accuracy of 10-20 nm while expected accuracy provided by the numerical simulations lies around 5-10 nm. A slight difference between the results obtained on the test bench and the numerical simulations then appears. More experimental measurements are required and are expected to be realized in 2014-2015 to understand the origin of this difference.

VI. ACKNOWLEDGEMENTS

VII. REFERENCES

[1] F. Roddier, *Curvature sensing and compensation: a new concept in adaptive optics*, Appl. Opt., 27 :1223–1225, (1988).
[2] R. Ragazzoni, *Pupil plane wavefront sensing with an oscillating prism*, J. of Modern Optics, 43 :289–293, (1996).
[3] J.-C. Fontanella, *Analyse de surface d'onde, déconvolution et optique adaptative*, J. Opt., vol. 16, 6, 257-268, (1985).
[4] R. A. Gonsalves, *Phase retrieval and diversity in adaptive optics*, Opt. Eng., 21 :829–832, (1982).
[5] V. Michau, G. Rousset, J.-C. Fontanella, *Wavefront sensing from extended sources*, in vol. 13 pp. 124–128 of NSO/SP Summer Workshop Series, Sunspot, New Mexico, USA, (1992).
[6] T. R. Rimmele, R. B. Dunn, and R. R. Radick, *Wavefront Sensing for Solar Adaptive Optics*, Bulletin of the American Astronomical Society, 28 :962, (1996).
[7] L. Poyneer, *Scene-based Shack-Hartmann wave-front sensing : analysis and simulation*, Appl. Opt., 42(29):5807–5815, (2003).
[8] T. R. Rimmele, *Recent advances in solar adaptive optics*, in Proc. SPIE 5490 pp. 34-46, (2004).
[9] C. Roddier, and F. Roddier, *Combined approach to the Hubble Space Telescope wave-front distortion analysis*, Appl. Opt. 32, 2992-3008 (1993).
[10] B. H. Dean, D. L. Aronstein, J. Scott Smith, R. Shiri and D. Scott Acton, *Phase retrieval algorithm for JWST Flight and Testbed Telescope*, Proc. SPIE 6265, 626511 (2006).
[11] L. Meynadier, *Analyse de surface d'onde pour le contrôle actif d'un télescope spatial*, Ph.D. dissertation, Université de Nice-Sophia Antipolis, Nice, France, (1997).
[12] F. Baron, I. Mocoeur, F. Cassaing, and L. M. Mugnier, *Unambiguous phase retrieval as a cophasing sensor for phased array telescopes*, J. Opt. Soc. Am. A **25**, 1000-1015 (2008).
[13] L. Meynadier, V. Michau, M.-T. Velluet, J.-M. Conan, L. M. Mugnier, and G. Rousset, *Noise Propagation in Wave-Front Sensing with Phase Diversity*, Appl. Opt. 38, 4967-4979 (1999).
[14] J. J. Dolne and H. B. Schall, *Cramer-Rao bound and phase-diversity blind deconvolution performance versus diversity polynomials*, Appl. Opt. 44, 6220-6227 (2005).
[15] A. Blanc, L. M. Mugnier, and J. Idier, *Marginal estimation of aberrations and image restoration by use of phase diversity*, J. Opt. Soc. Am. A 20, 1035-1045 (2003).
[16] I. Mocœur, L. M. Mugnier, and F. Cassaing, *Analytical solution to the phase-diversity problem for real-time wavefront sensing*, Opt. Lett. 34, 3487-3489 (2009).
[17] R. L. Kendrick, D. S. Acton, and A. L. Duncan, *Phase-diversity wave-front sensor for imaging systems*, Appl. Opt. 33, 6533-6546 (1994).
[18] A. Montmerle-Bonnefois, T. Fusco, S. Meimon, V. Michau, L. Mugnier, JF Sauvage, et al. *Comparative theoretical and experimental study of a Shack-Hartmann and a Phase-Diversity sensor; for high precision Wave-Front Sensing dedicated to space active optics*, this conference
[19] M. Laslandes, E. Hugot, M. Ferrari, C. Hourtoule, Ch. Singer, et al. *Mirror actively deformed and regulated for applications in space: design and performance*, Opt. Eng. 52(9), 091803 (2013).
[20] C. Engel, E. Hugot, M. Ferrari, C.Escolle, et al *The LAM space optics facilities*, this conference